NeuroImage 203 (2019) 116204

Contents lists available at ScienceDirect

NeuroImage

journal homepage: www.elsevier.com/locate/neuroimage

Semantic and perceptual priming activate partially overlapping brain networks as revealed by direct cortical recordings in humans

Elvira Khachatryan [a,*], Benjamin Wittevrongel [a,1], Mansoureh Fahimi Hnazaee [a], Evelien Carrette [b], Ine Dauwe [b], Alfred Meurs [b], Paul Boon [b], Dirk van Roost [c], Marc M. Van Hulle [a]

[a] Laboratory of Neuro- and Psychophysiology, KU Leuven, Heresstraat 49, B-3000, Leuven, Belgium
[b] Laboratory of Clinical and Experimental Neurophysiology, Neurology Department, Ghent University Hospital, De Pintelaan 185, 9000, Ghent, Belgium
[c] Department of Neurosurgery, Ghent University Hospital, De Pintelaan 185, 9000, Ghent, Belgium

ARTICLE INFO

Keywords:
Invasive EEG
Perceptual priming
Semantic priming
Object processing
Spatio-temporal dynamics

ABSTRACT

Facilitation of object processing in the brain due to a related context (priming) can be influenced by both semantic connections and perceptual similarity. It is thus important to discern these two when evaluating the spatio-temporal dynamics of primed object processing. The repetition-priming paradigm frequently used to study perceptual priming is, however, unable to differentiate between the mentioned priming effects, possibly leading to confounded results. In the current study, we recorded brain signals from the scalp and cerebral convexity of nine patients with refractory epilepsy in response to related and unrelated image-pairs, all of which shared perceptual features while only related ones had a semantic connection. While previous studies employing a repetition-priming paradigm observed largely overlapping networks between semantic and perceptual priming effects, our results suggest that this overlap is only partial (both temporally and spatially). These findings stress the importance of controlling for perceptual features when studying semantic priming.

1. Introduction

Visual object processing and recognition is considered to primarily develop along the ventral stream of human and primate brains starting from the primary visual cortex (V1) and onwards to the inferior temporal areas (Kravitz et al., 2013). This process also involves parts of the dorsal stream, such as anterior temporal and frontal areas. The activation in these anterior areas was shown to be influenced by the conducted task (Harel et al., 2014), experimental design (Thoma and Henson, 2011) and the context in which the object is presented (Bar and Aminoff, 2003; Riès et al., 2017). The effect of context is specifically essential when studying object processing since in natural conditions objects are rarely presented in isolation. A related context normally facilitates object processing (priming), as reflected by faster reaction times in behavioral studies (Hart and Reeve, 2007), decreased activation of certain brain areas in fMRI studies (Tivarus et al., 2007) and decreased amplitude of certain time-locked EEG deflections (event-related potentials, ERPs) (Khachatryan et al., 2016a; Van Vliet et al., 2014).

Studies on scalp-recorded EEG suggest that the effect of a related context comes into play at around 400 ms (N400 ERP) after presenting the target object (Khachatryan et al., 2016a; Kovalenko et al., 2012). Recently, it has been shown (Xu et al., 2012; Coulson et al., 2005), that this effect can start even earlier (around 200 ms). As to the spatial distribution of the said effect, some studies suggest the involvement of a large number of brain areas, including the occipito-temporal cortex, posterior parietal cortex and prefrontal cortex (Badgaiyan, 2000; Mummery et al., 1999; James et al., 2000), while others propose a more localized distribution, mainly in the left temporal cortex (Rossell et al., 2003; Patterson et al., 2007). Although, the techniques used in these studies (scalp-recorded EEG or fMRI) provide insight into the temporal and spatial aspects of object priming, they fall short in revealing both simultaneously. While fMRI yields a superior spatial resolution (1 cm), it lacks temporal precision and, conversely, scalp-EEG offers millisecond temporal resolution but compromises on spatial precision. In an effort to investigate the spatio-temporal dynamics of object priming, James et al. (2000) developed an fMRI experiment with a gradual unmasking of the visual stimuli over a period of 46 s, which allowed them to observe brain processes before and after recognition of the target object. Even though

* Corresponding author.
E-mail address: Elvira.Khachatryan@kuleuven.be (E. Khachatryan).
[1] Shared first co-author.

https://doi.org/10.1016/j.neuroimage.2019.116204
Received 21 December 2018; Received in revised form 19 August 2019; Accepted 17 September 2019
Available online 17 September 2019

this method yielded an advantage over previous neuroimaging studies, one should be careful when comparing their results to those of ERP studies, as it has been recently shown that the BOLD signal, as measured with fMRI, positively correlates with high frequency rhythms (high--gamma), instead of ERP responses (Haufe et al., 2018) that typically comprise lower-frequency components (Luck, 2005). Furthermore, in natural settings, object recognition and its consecutive modulation by available context (priming) occur within milliseconds. Thus, when postponing the recognition of the object, it is not clear that one would observe the same activations as during natural object recognition. In order to evaluate the spatio-temporal dynamics of natural object priming, a technique is needed that reconciles both resolutions, such as intracranial EEG (iEEG). Electrocorticography (ECoG) is a type of iEEG that records brain activity directly from the cortical surface and yields excellent signal-to-noise ratio, is less affected by signal mixing due to volume conduction and captures also high-frequency rhythms (above 80 Hz) (Parvizi and Kastner, 2018). Only a handful of studies investigated the priming effect using intracranial EEG. For instance, in a recent iEEG study, that used a blocked-cyclic picture-naming paradigm, Ries et al. (Riès et al., 2017) located word-retrieval and selection (as an indicator of lexico-semantic processing in language production) in the fronto-temporal system. They showed that these processes were temporally widespread. The authors considered a type of repetition priming paradigm, commonly used to gauge language production and semantic priming effects. However, as this paradigm fails to control for visual similarity (perceptual priming), it is difficult to make claims about actual semantic priming, since similar to other repetition paradigms, it evokes both semantic (associative) and perceptual (similarity) priming effects. Hence, it is still an unresolved question whether and if yes, to which extent the perceptual and semantic priming effects overlap during object processing in spatial and/or temporal domains (Binder et al., 2009).

In the current study, we set out to tease apart the effects of semantic and perceptual priming in both the spatial and temporal domains. We will do this by recording ECoG in response to 200 related and 200 unrelated image-pairs taken from the POPORO image database (Kovalenko et al., 2012) using a delayed semantic judgment task. The images in this database are controlled for a number of low-level visual characteristics such as luminescence, skewness, etc, as well as, color, shape and size between prime and target images. In this way, we can control the prime (first) and target (second) images for visual similarity. Hence, if related and unrelated target images differently modulate the recorded signal, we can reliably assume it to be due to a difference in semantic rather than perceptual priming. In the same vein, we can compare prime and unrelated target responses to investigate the effect of pure perceptual priming.

We first analyze scalp-recorded EEG to show the temporal dynamics of semantic- and perceptual-priming, after which we investigate their spatiotemporal dynamics using different ECoG signal characteristics.

2. Results

2.1. Behavioral results

The average performance accuracy on the task is 0.89 (0.86 for related and 0.93 for unrelated image-pairs). The Kruskal-Wallis non-parametric test with relatedness as a fixed effect shows a significant difference between these performance accuracies ($\chi 2\ (1,\ 16) = 7.27$, $p = 0.007$).

2.2. Scalp-recorded EEG

Since intracranial recordings serve primarily clinical purposes such as functional mapping of eloquent cortex or detection of the seizure-onset zone in drug-resistant epilepsy patients, scalp-EEGs of quality sufficient for research purposes that are simultaneously recorded with intracranial EEGs are rarely available. The long-term monitoring sessions of such patients, required for their diagnostic workup, eventually can lead to conductive gel dry-out. This, together with the hair grow in the electrode location, negatively affects the quality of the recorded scalp EEG. Careful adjustment prior to the experimental sessions, follow-up of the scalp-EEG quality, and, careful selection of the scalp electrodes during the analysis provide us with the opportunity to arrive at recordings that exhibited relatively little influence from the aforementioned factors. The medical personnel did their best not to deviate much from the established 10–20 system when fixating electrodes on the scalp. However, in case when the scar would coincide or be too close to an established electrode position from 10/20 system, the electrode was slightly deviated in order to avoid contamination of the scar with the used glue. These deviations never exceeded a few cm. Additionally, since in our study, we do not rely on the spatial resolution of our recorded scalp EEG, we are confident that these slight deviations do not affect our conclusions.

Despite the efforts of the medical staff, the scalp-recorded EEG of patients P2 and P3 had to be excluded as the signal quality was poor.

We conduct the Kruskal-Wallis test with stimulus type (prime, related and unrelated targets) as a fixed effect on the ERP responses of remaining 22 scalp-EEG electrodes from the initially recorded 27, in order to evaluate the temporal dynamics of perceptual and semantic priming (Fig. S4 in Supporting Information (SI)) and further compare these results with the ones obtained from intracranial recordings. It shows a significance for N100 (e.g., for electrode Oz, $\chi^2\ (2, 3265) = 10.87$, $p = 0.0044$) and P200 (e.g., for electrode Oz, $\chi^2\ (2, 3265) = 14$, $p = 0.0009$) on very few electrodes. For the later ERP components (N400 and P600) the effect is more widespread and pronounced (e.g., for electrode Cz, $p \ll 0.0001$, for both N400 and P600).

Afterwards, during multiple comparisons with FDR correction we compare three pairs of stimuli: related vs. unrelated targets (Rel→Unrel), prime vs. related targets (Prime→Rel) and, prime vs. unrelated targets (Prime→Unrel). The results (Fig. 1) reveal significantly more negative N100 for prime stimuli compared to both target stimuli (on electrode O1, $\chi^2\ (1, 2468) = 5.45$, $p_{cor.} = 0.02$ for Prime→Rel., and $\chi^2\ (1, 2496) = 7.79$ $p_{cor.} = 0.0052$ for Prime→Unrel.). For P200, both target stimuli (related and unrelated) evoke a significantly larger positivity compared to the prime stimuli on a few electrodes (e.g., on electrode Oz, $\chi^2\ (1, 2459) = 3.97$, $p_{cor.} < 0.05$ for related and $\chi^2\ (1,\ 2481) = 13.3$, $p_{cor.} = 0.0003$ for unrelated targets). No significant difference between related and unrelated targets is observed in these early time windows. As to the N400 window, the related target evokes significantly less negativity compared to both unrelated target and prime stimuli (for electrode Cz, $p_{cor.} < 0.0005$ for both comparisons). Unrelated targets evoke an N400 with a significantly smaller amplitude compared to the primes (for electrode Cz, $\chi^2\ (1, 2509) = 5.07$, $p_{cor.} = 0.024$). During the P600 time-window, similar to N400, all three stimulus groups differ. Here, both target groups evoke a significantly larger P600 compared to the prime (in both cases $p_{cor.} \ll 0.001$) (Fig. 1). During this time interval, the difference between related and unrelated targets is present mainly on centrally located electrodes (e.g., for electrode Pz, $\chi^2\ (1,\ 1529) = 5.05$, $p_{cor.} = 0.025$). The FDR-corrected p-values for multiple comparison for each scalp electrode that shows significance can be found in the SI, arranged according to the investigated ERPs (Table S2).

In summary, in scalp-recorded EEGs, the effect of perceptual priming is noticeable already in early time windows (N100 and P200) while the effect of semantic priming is present in later (N400 and P600) time windows only.

2.3. Intracranial EEG

In order to arrive at a complete picture of the spatiotemporal dynamics of perceptual and semantic priming, we conduct three types of analysis on each recorded ECoG electrode (for locations of the electrodes, see SI, Table S3, and Fig. S1; for the MNI coordinates of each electrode, see SI, Table S4). First, we conduct the ERP analysis that has been long considered for studying the temporal dynamics of priming in both scalp-

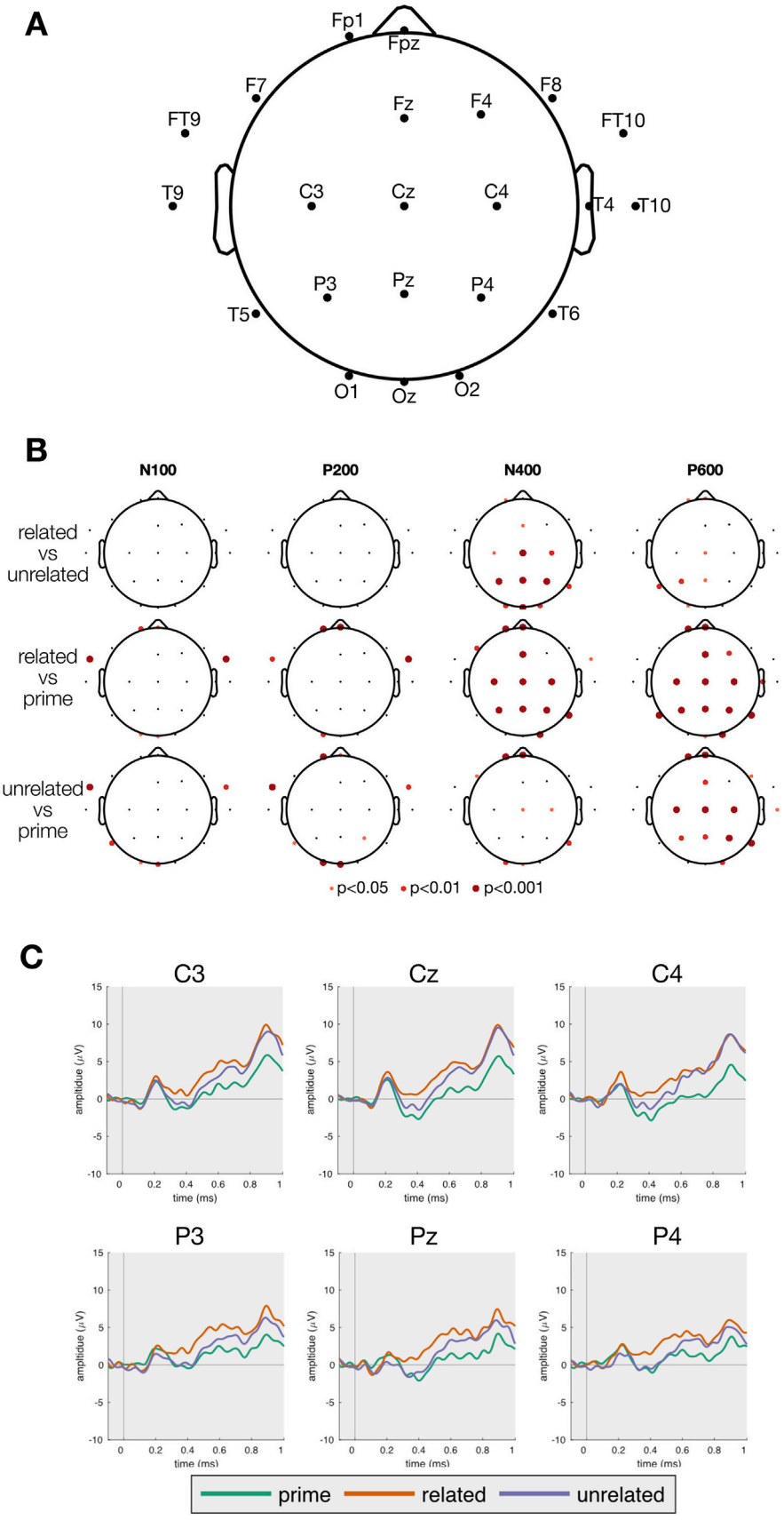

Fig. 1. Spatial (panel B) and temporal (panel C) overview of perceptual and semantic priming effects from the scalp-recorded EEG. Each dot in the panel B represents an electrode location with its according statistics. The panel A represents the names and the locations of the studied electrodes.

recorded (Khachatryan et al., 2016a; Kovalenko et al., 2012) and intracranial EEG (Nobre and McCarthy, 1995; Khachatryan et al., 2016b, 2018). After that, we conduct a time-frequency analysis looking for event-related synchronization/desynchronization (ERS/ERD) in the high-gamma (80–120 Hz), alpha (8–12 Hz) and theta (4–7.5 Hz) bands, each of which reflects certain conditions (e.g., focal activation for high-gammas) in the brain. Finally, in order to show that it is possible to discriminate between our stimulus groups (prime, related target and unrelated target) on a single-trial level, for certain brain areas, we conduct a classification analysis.

2.3.1. ERP analysis

For the intracranial electrodes, the Kruskal-Wallis test with the effect of stimulus type (a difference between any of three types of stimulus groups) is both temporally and spatially widespread. Depending on the location of the grid, each subject has between 30% and 94% electrodes with a significant effect of stimulus type for any of four ERP components with average value 64.1% after removing the contaminated electrodes.

For ERP analysis only, the statistical analysis is conducted between prime and target stimuli with the ratio of 2:1, as in general the number of prime stimuli is twice that of individual target stimuli (related or unrelated). Furthermore, depending on the number of contaminated trials, different subjects ended up with a different number of trials that entered the statistical analysis. By conducting an additional bootstrapping analysis with one of the grids over the left temporal cortex (patient P1, SI, Table S3) we show that our results are not significantly affected by the amount of data entering statistical analysis and that even the limited amount of data (i.e., patient P9) presented in the current paper is sufficient to draw reasonable conclusions. For details of the analysis and the results, we refer the reader to SI.

Early object processing affected by semantic priming: Visual inspection of ERPs from retained electrodes shows pronounced early ERP components (N100 and P200) on grids covering the right posterior basal and lateral occipitotemporal cortices (Fig. 2A, left panel) for all stimulus groups. Unlike scalp-recorded EEG, here, multiple comparison with FDR correction reveals a difference between related and unrelated targets

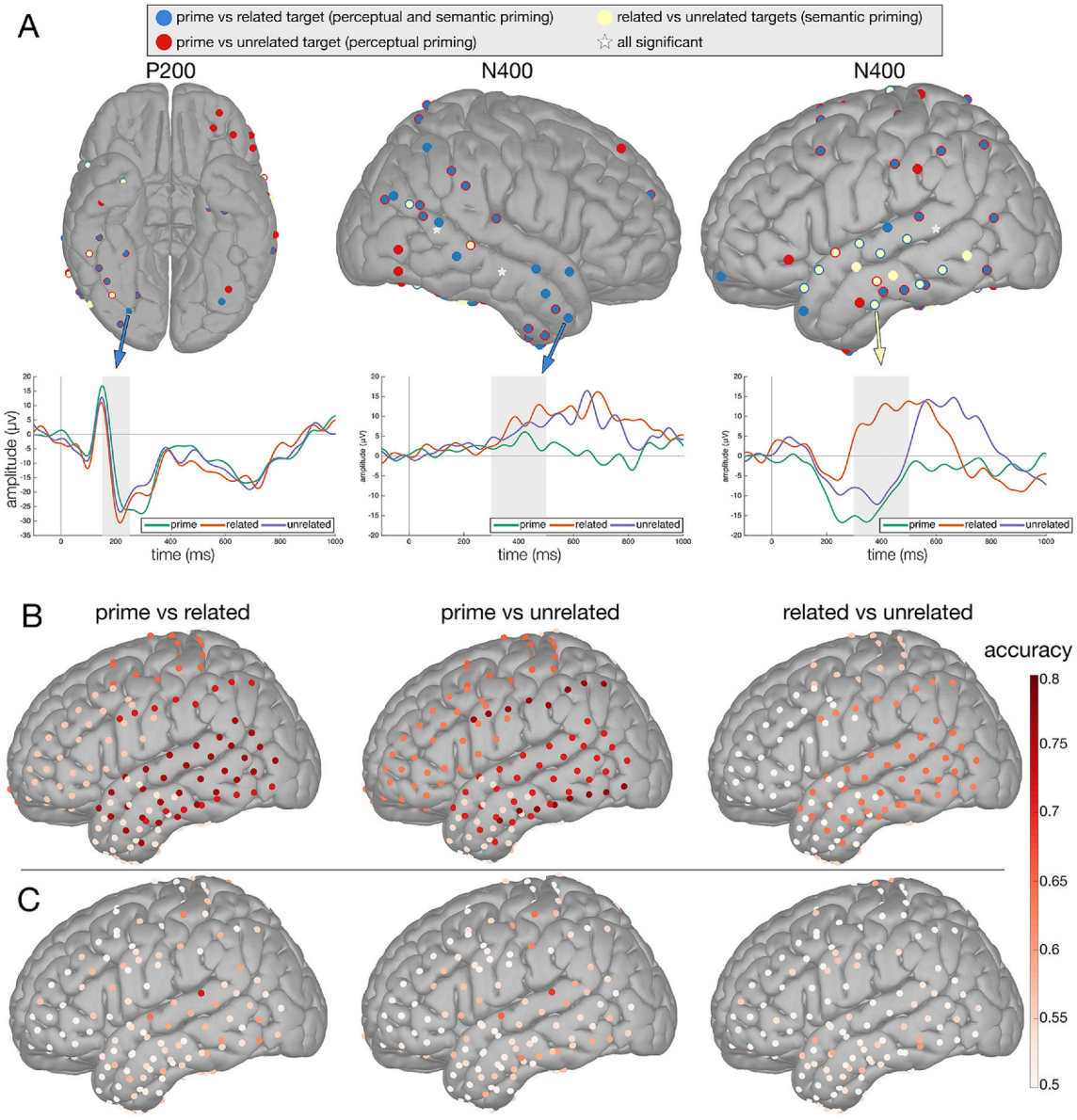

Fig. 2. Spatial and temporal distribution of semantic and perceptual priming effects in ERP (panel A), and results for multichannel (panel B) and single-channel (panel C) classification analysis. Colormap represents the accuracy values for both single- and multichannel classification. The electrodes are presented on the icbm template. We refer the reader to SI (Table S4) for MNI coordinates of individual electrode.

during both the N100 and P200 time windows (Fig. 2A, left panel and Fig. S5 in SI) over the right lateral (for N100, χ^2 (1, 394) = 6.22, $p_{cor.}$ = 0.037 and for P200, χ^2 (1, 394) = 9.01, $p_{cor.}$ = 0.004) and basal (for N100, χ^2 (1, 136) = 11.7, $p_{cor.}$ = 0.0019 and for P200, χ^2 (1, 136) = 7.88, $p_{cor.}$ = 0.015) occipitotemporal cortices. The difference between related targets and primes representing the combination of perceptual and semantic priming, as well as between unrelated targets and prime, representing purely perceptual priming, are already evident in the early time-windows (N100 and P200) in the lateral and basal occipitotemporal areas on both hemispheres ($p_{cor.}$ <0.05) (Fig. 2A, left panel and Fig. S5 in SI). Unlike the former, the latter comparison involves left basal frontal (Fig. 2A) (e.g., for N100, χ^2 (1, 292) = 8.7, $p_{cor.}$ = 0.0095) and inferior parietal lobes (for N100, χ^2 (1, 299) = 8.05, $p_{cor.}$ = 0.014).

Perceptual and semantic priming affect both hemispheres in later time-windows: During N400 and P600 time-windows, the semantic priming (Rel→Unrel) is present in the temporo-basal (Fig. S5, in SI) and lateral temporal cortices of both hemispheres (Fig. 2A, central and right panels). This effect is most pronounced in the left superior and middle temporal gyri (Fig. 2A, right panel) (for N400 on superior temporal gyrus, χ^2 (1, 394) = 17.89, $p_{cor.}$ = 0.0019; for P600 on the middle temporal gyrus (χ^2 (1, 394) = 17.3, $p_{cor.}$ = 0.0013). In these time windows, the Prime→Rel difference, similar to the Prime→Unrel difference, becomes more pronounced and widespread (Fig. 2A), including the more anterior parts of mainly the right (e.g., for N400, in the right anterior temporal lobe χ^2 (1, 508) = 8.22, $p_{cor.}$ = 0.02), but also the left temporal cortices and the left superior frontal (for P600, χ^2 (1, 258) = 34.47, $p_{cor.}$<0.0001) and right prefrontal (for P600) cortices (χ^2 (1, 205) = 16.24, $p_{cor.}$ = 0.00017). Interestingly, the early involvement of the left basal frontal cortex in the Prime→Unrel comparison disappears in later time windows (N400 or P600) (Fig. S5 in SI).

In summary, the ERP analysis of intracranial recordings suggests that the processing of perceptual and semantic priming occur in partially (both spatially and temporally) overlapping networks, with semantic priming concentrated more in the left temporal cortex and culminating later in time, while perceptual priming is widespread already in early time windows.

2.3.2. Time-frequency (ERS/ERD) analysis

The intracranial recordings give us the opportunity to investigate the higher frequency bands (>80Hz) that bear additional information about the brain functions (Crone et al., 2006). However, to perform an ERP analysis, we need to filter the signal in the lower frequency ranges (e.g., <30 Hz), thus, losing a considerable amount of valuable information. Furthermore, it has been shown that different frequency bands carry different types of information, including local neuronal activation for high gammas (Crone et al., 2006), active inhibition (Klimesch, 2012) or disengagement (Infarinato et al., 2015) for alpha and, selective attention processing (Basar-Eroglu et al., 1992) and expectations (Başar, 1999) for theta bands. These bands are often linked to object recognition (Riès et al., 2017; Rupp et al., 2017; Martinovic et al., 2012) and priming (Harel et al., 2014; Mellema et al., 2013) in different modalities, and have relatively clear cognitive processes assigned to them (see above). Furthermore, in our previous work we showed that these bands are actively involved in the basic visual processing (Wittevrongel et al., 2018a). Therefore, in order to evaluate these processes, we conducted ERS/ERD analysis on intracranial recordings in the mentioned three frequency bands: high gamma (80–120 Hz), alpha (8–12 Hz) and theta (4–7.5 Hz). The increase in frequency power compared to the baseline is referred to as ERS, while the decrease is referred to as ERD.

Opposite high-gamma (80 – 120 Hz) power modulation in left temporal cortex for primes and for both targets (Fig. 3, upper panel): For each stimulus type, the significant ERS for the high gamma band is observed for the electrodes covering the lateral and basal occipitotemporal cortices (Fig. S6 in SI) mainly on the right hemisphere starting at around 100 ms post-onset and lasting until the end of the epoch. Left lateral temporal cortex (mainly middle and inferior temporal gyri) showed ERS for both target groups (average power change across time (APC) = 5.55, CI = [3.22, 9.01] for related and APC = 4.42, CI = [2.24, 7.75] for unrelated targets respectively) with considerably less activation for the unrelated group starting from around 300 ms post-onset, and ERD for prime stimuli (APC = −0.56, CI = [-0.77, −0.25]) (Fig. 3, upper panel). Right prefrontal cortex shows an ERS in response to primes (APC = 2.20, CI = [1.32, 3.60]) and related targets (APC = 0.25, CI = [0.02, 0.68]), but not in response to unrelated targets (Fig. S6 in SI). Noticeably, more

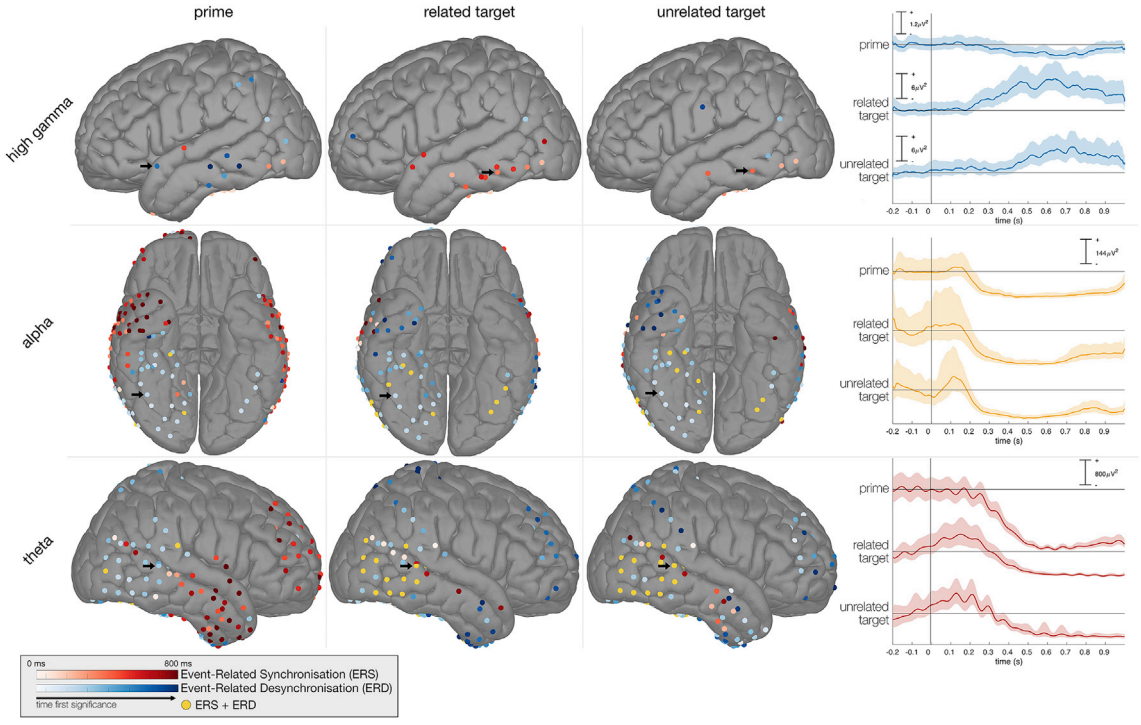

Fig. 3. Time-frequency analysis for high-gamma, alpha and theta bands. Arrows show the location of the electrodes, of which the temporal patterns (right column) are shown. The electrodes are presented on the icbm template. We refer the reader to SI (Table S4) for MNI coordinates of individual electrode.

anterior brain areas express a change in high gamma power (ERS/ERD) in later time windows compared to posterior areas.

Object processing evokes ERD in alpha band (8 – 12 Hz) in the right basal occipitotemporal cortex independently of the presence of context (Fig. 3, middle panel): For this frequency band, in the right lateral (starting around 250 ± 50 ms post-onset) and basal (posteriorly starting around 200 ms and anteriorly – around 350 ms) occipitotemporal cortex, the alpha band exhibits significant ERDs (Fig. 3, middle panel) in response to all stimulus groups (e.g., for prime in lateral posterior temporal cortex, APC = −323.07, CI = [-338.02, −302.38]), while on very few electrodes mainly in response to targets, this ERD is preceded by an early ERS (ERS-ERD complex). In the right prefrontal (starting from around 600 ms) and mainly the left superior parietal cortices (starting from around 470 ms), significant ERSs are observed in response to primes (e.g., for prefrontal cortex APC = 5.24, CI = [1.72, 10.98]), while ERDs are observed for both target groups (APC = −16.32, CI = [-24.16, −1.15] for related and APC = −6.12, CI = [-9.02, −1.01], for unrelated) (Fig. S7 in SI). In the left temporal lobe, primes evoke a widespread ERS (APC = 9.55, CI = [3.02, 19.01]) starting from 450 ± 50 ms. Here, the related targets evoke an ERD mainly in the middle temporal gyrus (APC = −119.50, CI = [-158.43, −66.13]), while unrelated targets evoke both ERD (APC = −264.47, CI = [-313.84, −186.9]) and ERS (APC = 7.79, CI = [1.12, 16.7]). In the right anterior temporal cortex (Fig. S7 in SI), prime (APC = 42.63, CI = 7.13, 106.35]) and related target (APC = 57.65, CI = [12.92, 156.25]) evoke an ERS starting from around 400 ms albeit the latter one to the lesser degree. Here (mainly in the temporal pole), the unrelated targets mainly evoke an ERD (APC = −114.67, CI = [-152.99, −33.24]).

Differential modulation of theta-band (4 – 7.5 Hz) power in right lateral temporal and frontal cortices in response to objects with and without context (Fig. 3, lower panel): For this frequency band, certain brain areas show a common behavior for all three stimulus groups, while others show a differential behavior for prime and target stimuli. For instance, all three stimulus groups evoke ERDs in the right basal occipitotemporal cortex (e.g., for the prime stimulus, APC = −225.43, CI = [-254.47, −177.61]) starting around 250 ms post-onset with occasional ERS-ERD complexes (Fig. S8 in SI). The right superior parietal cortex shows significant ERDs (for prime, APC = −101.35, CI = [-120.24, −59.03]; for related target, APC = −55.43, CI = [-69.77, −15.63]; and for unrelated target, APC = −87.99, CI = [-111.18 -29.88]) starting around 350 ms post-onset, while the left superior and middle temporal gyri show significant ERSs (for prime, APC = 28.08, CI = [12.58, 50.60]; for related target, APC = 48.40, CI = [5.79, 137.53]; for unrelated target, APC = 24.91, CI = [8.15, 48.56]) starting from around 450–500 ms post-onset in response to all stimulus groups (Fig. S8 in SI). On the other hand, in the right lateral occipitotemporal cortex, ERD is observed in response to prime (APC = −418.46, CI = [-494.04, −314.33]), while ERS-ERD complex in response to both target groups (Fig. 3, lower panel). Furthermore, in the right anterior temporal- (around 500 ms), and prefrontal cortices (around 600 ms post-onset), significant ERS is observed in response to prime (e.g., for prefrontal cortex, APC = 67.35, CI = [46.60, 95.83) stimuli and ERDs in response to both target stimulus groups (APC = −30.02, CI = [-35.58, −19.34] for related, and APC = −27.5, CI = [-34.76, −14.64] for unrelated target).

In summary, the ERS/ERD analysis shows an early engagement of (mainly) right basal occipitotemporal cortex (ERS in high-gamma and ERD in alpha) during object processing independently of the presence or absence of a context. On the other hand, the left temporal cortex is engaged in processing of both semantic and perceptual priming (the latter one to a lesser degree) around the time when semantic processing takes place (Halgren et al., 1994), while the right temporal cortex exhibits mainly facilitation during perceptual priming.

2.3.3. Classification analysis

Single-trial based discrimination between stimulus groups is possible (Fig. 2B and C and, Fig. S9 in SI): The classification analysis of each individual channel using the entire 1 s ERP epochs indicates the possibility to discriminate (on a single-trial basis) between prime and target groups with a maximal accuracy of about 70% (72.03% between prime and related targets, and 68.48% between prime and unrelated targets, respectively), and between related and unrelated target groups with 61.08% accuracy (Fig. 2C). Interestingly, when including data from the entire grid, the accuracy reaches 64.04% for the discrimination between related and unrelated target images and more than 75% for the discrimination between prime and target images (prime versus related target 75.99%, prime versus unrelated target 77.21%). Given the importance of the left temporal cortex in semantic processing, it is not surprising to see that the grid over this area shows the highest accuracy (Fig. 2B). These accuracy values are significantly above chance level and are comparable with the ones from previous literature (Rupp et al., 2017).

3. Discussion

The main objective of our study was to evaluate the spatiotemporal dynamics of perceptual and semantic priming effects on visual object processing and to discern these effects in both temporal and spatial domains. We investigated both scalp and intracranial responses and conducted ERP, ERS/ERD and classification analyses on intracranial data.

3.1. The difference in spatiotemporal dynamics of semantic and perceptual priming effects

Similar to some previous studies in our scalp-recorded EEG we observed the effect of perceptual priming (the difference between primes and unrelated targets) in early ERP components, while the semantic priming (the difference between related and unrelated targets) was present starting from the N400 time-window (Kovalenko et al., 2012; Zhanga et al., 1997), that is believed to reflect the semantic processing of a presented object (Kutas and Federmeier, 2011). On the other hand, the ERP results of our intracranial recordings showed that both perceptual and semantic priming affect object processing in the early stages. Some early scalp-ERP studies also suggest access to semantic information during early visual processing (Proverbio et al., 2007). The fact that we did not observe it in our scalp-recorded EEG can probably be due to the small effect of semantic priming in early time windows. In ECoG, the said effect was most pronounced in later time-windows (in particular during the N400) and was spatially localized mainly in the left superior and middle temporal gyri and, to a considerably lesser extent, in the right temporal cortex (middle temporal and fusiform gyri). This observation suggests that semantic priming reflected by the N400 ERP is mainly concentrated in the left temporal cortex, as previously reported (Khachatryan et al., 2018; Ghosh Hajra et al., 2018).

Pure perceptual priming, on the other hand, is more widespread during early time-windows compared to semantic priming, spanning the right ventral stream (basal and lateral occipitotemporal cortex) and left inferior parietal and basal frontal cortices. Remarkably, the activation of the latter completely disappears in the late time windows (N400 and P600). In general, the effect of perceptual priming, similar to that of semantic priming, culminates during later time-windows by including both frontotemporal networks. This spread of visual feature processing across the cerebral cortex was recently shown in the study by Rupp et al. (2017) where they were able to categorize objects with relatively high accuracy (67%) based on ECoG data and by incorporating different features of the categories (e.g., airplanes have wings). Furthermore, Ries et al. (Riès et al., 2017) described a broad involvement of the left frontotemporal network in the processing of a repeated stimulus. Our results suggest that this broad involvement can be due to the existing perceptual priming since their study did not account for the possible confusion between perceptual and semantic priming, which is inevitable in case one adopts a repetition priming paradigm. Our results, together with the aforementioned studies reveal the complex dynamics of perceptual and semantic priming on object processing.

3.2. Time-frequency analysis reveals the effect of context on object processing

High gamma (ERS/ERD) is the most commonly investigated band in the ECoG studies (Crone et al., 2006). The increase in its power reflects a local activation and engagement of certain brain areas, whereas its decrease reflects inhibition or disengagement (Miller et al., 2009; Towle et al., 2008). The modulation of high gamma power was observed to be widespread over the cerebral cortex in response to repetition priming paradigm (Riès et al., 2017), to be located in left posterior parietal cortex in response to recognition memory decision paradigm (Gonzalez et al., 2015) and in the left inferior frontal cortex in response to overt object naming task (Babajani-feremi et al., 2016).

Our results showed that both prime and target images evoked an increase in high-gamma band power in the right lateral and bihemispheric basal occipitotemporal cortices starting early after stimulus-onset and lasting throughout the entire processing (1s epoch) indicating the involvement of these brain areas during the entire course of object processing. The involvement of the basal temporal cortex in processing meaningful stimuli was previously shown using words (Thesen et al., 2012) and images (Rangarajan et al., 2014; Kapeller et al., 2018). Our thorough analysis of the temporal aspects of object processing suggests that semantic processing occurring in the basal occipitotemporal cortex starts early on after stimulus presentation. The anterior parts of lateral temporal cortices, however, start their involvement at a later stage (about 400 ms) around the time when context can influence object processing (priming) (Kutas and Federmeier, 2009). It is noteworthy that we observe a decrease in high-gamma power (ERD) in the middle left temporal gyrus in response to primes, while its power increases in response to targets (particularly related targets). This leads us to hypothesize that the left middle/inferior temporal gyri are inhibited or disengaged (Towle et al., 2008) when processing an object without context, while the same areas are activated when a semantically related context is added. This is additionally supported by the observed ERSs in the alpha band during the said time windows in response to primes and ERDs in response to related targets, as an increase in alpha power has been linked to inhibition (Klimesch, 2012). Some previous studies (Khachatryan et al., 2018; Migliaccio et al., 2016) suggest the involvement of the middle part of the left middle temporal gyrus (mMTG) in semantic processing and locate the semantic hub in the anterior temporal cortex (ATL) (Patterson et al., 2007), also based on observations of N400 in that area (Lau et al., 2013; Jackson et al., 2015). In the current study, we observed an N400 effect in the left middle temporal cortex spanning to ATL, as well as an increase in high-gamma power around the N400 time window in response to related targets, which confirms the involvement of this area in semantic processing. However, we assume that these observations are indicators of major influence of context on object processing, rather than indicators of semantic processing of a stand-alone object since it was not observed for the prime stimuli. On the other hand, all three image groups showed an increase in high-gamma and a decrease in alpha power in posterior lateral temporal cortex starting from around 250 ms post-onset, which can support the hypothesis that the posterior temporal cortex (pMTG particularly) could serve as a semantic hub (Brouwer and Hoeks, 2013). Furthermore, the observed ERSs in alpha band in response to primes and ERDs in response to both targets in the anterior regions suggest that processing of objects mainly occur in the ventral stream (Devereux et al., 2018), while the anterior brain regions are more engaged in the processing of priming (Bar and Aminoff, 2003; Riès et al., 2017), the imposed task (Harel et al., 2014), feedback and cognitive control (Thoma and Henson, 2011).

Similar to the alpha band, we observed a spatially widespread modulation in the theta band in response to our image groups. Previously, this modulation has been shown in the context of visual stimulus processing (Gevins et al., 1997) and, depending on the location, suggested to be a biomarker of working memory (Martinovic et al., 2012; Gevins et al., 1997), semantic retrieval (Bastiaansen et al., 2008), episodic retrieval (for a review see Nyhus and Curran (2010)) and, preparation and planning (Tomassini et al., 2017). Given the wide spectrum of functions assigned to this band, its observed widespread modulation is not surprising, especially when using complex visual stimuli, as in our study. The observed increase in theta band power followed by a decrease in the right basal temporooccipital cortex for all image groups can be an indicator of semantic retrieval followed by further integration. Interestingly, in the right lateral occipitotemporal cortex, this pattern of theta band modulation was observed only for the two target groups, which can be explained by the effect of primed targets on working memory since this brain area was shown to be involved in encoding and maintenance of spatial representations in humans (Berman and Colby, 2002). This suggestion is further confirmed by the observed ERS in response to the prime and ERD in response to both target groups in the right prefrontal cortex. This indicates a lower working memory load for the primed target stimuli compared to the stand-alone prime stimuli (Heyman et al., 2015; Sabb et al., 2007).

3.3. General discussion

The idea of discerning semantic and perceptual priming effects has been lingering in the scientific community for more than a decade. However, given the labor-intensive process of matching the objects for the similarity, a number of studies employed an approach that differs from ours. These studies (scalp-EEG (Xu et al., 2012; Kiefer, 2001) and fMRI (Lucia et al., 2010; Schacter et al., 2004; Eddy et al., 2007)) used paradigms with repetition of identical or different exemplars from the same category. However, given that the different exemplars from the same category share visual features, which has been shown recently to be useful for discrimination between categories (Rupp et al., 2017), using this strategy, it is not possible to completely discern responses to semantic and perceptual priming. Using the opposite strategy (similar un-related objects), we managed to discern between these two types of priming. A study from De Lucia et al. (2010), attempted to discern the effects of semantic and perceptual priming for the auditory modality using fMRI. They found a similar repetition suppression in the frontotemporal network in response to repetition of identical sounds and of a different sound from the same category (e.g., different sounds from a violin), from which they concluded that perceptual and semantic priming effects share the same spatial distribution. Our findings contradict this claim, as in our case the effect of perceptual priming was more widespread compared to the effect of semantic priming. De Lucia et al. (2010), similar to previous studies on the visual modality (for review, see Di Carlo et al. (DiCarlo et al., 2012)), used (identical) repetition of a presented sound as an indicator of perceptual priming, thus, they were unable to achieve pure perceptual priming, which would be lacking a semantic priming component. In our case, we achieved pure perceptual priming by using unrelated image pairs that shared perceptual features only (Kovalenko et al., 2012). Therefore, we suggest that our results provide a new and reliable insight into the spatiotemporal dynamics of pure perceptual and semantic priming effects. Our additional classification analysis confirmed the robustness of our results and proved that we can discern the above-mentioned effects on a single trial level. Unlike previous studies (Riès et al., 2017; Rupp et al., 2017) that used high gamma band activity, we conducted the classification on the ERPs and obtained relatively high accuracies (up to 77% for perceptual and 64% for semantic priming).

4. Conclusion

In our study, we were able to discern between semantic and perceptual priming effects during visual object processing in both temporal and spatial domains, using ERP and time-frequency analyses of intracranial recordings. We showed that these two types of priming occur in partially overlapping networks, with semantic priming being more constrained to the left temporal cortex and culminating later in time, whereas

perceptual priming starts at an earlier stage of visual object processing and is more widespread along the ventral stream as well as the fronto-temporal network.

5. Methods and materials

5.1. Participants

Nine patients with refractory epilepsy (4 females, average age 38.7 (std = 16.7) years, two left-handed) participated in the study. They were implanted with subdural (ECoG) and depth EEG electrodes for invasive video-EEG monitoring at Ghent University Hospital. Their demographic and clinical characteristics are listed in Table S1 in SI. All patients had normal or corrected to normal vision and normal level of consciousness. The study was conducted according to the current version of the Declaration of Helsinki (2013), following ethical approval from Ghent University Hospital's Ethics Committee. All participants gave their written informed consent prior to participating in the study and after being informed about the experiment and its goal.

5.2. Materials

Two hundred related and 200 unrelated pairs of images (400 x 400 pixel size) were taken from the POPORO database (Kovalenko et al., 2012). The stimuli were color images of real-life objects with no background. The set was composed of the images of animals, flowers and trees, foods, vehicles, clothing, household items, kitchen and office appliances, sports and medical equipment, etc. The images were balanced on a number of low-level characteristics: a two-tailed Student's t-test, with additional Satterthwaite's correction, where necessary, did not indicate any statistically significant difference between kurtosis ($t(1, 199) = 1.45$, $p = 0.15$), luminance ($t(1, 199) = 0.12$, $p = 0.9$) and skewness ($t(1, 199) = 0.4$, $p = 0.69$) between related and unrelated image groups. Furthermore, the authors of the database ascertained themselves for the visual similarity between prime and target images, so that they mainly differ by their semantics. Additionally, participants of the study on the development of the used database (Kovalenko et al., 2012) confirmed that they recognize all the images in the final published dataset. The subset of the database used in the current study can be accessed from the following source: https://kuleuven.box.com/v/Kovalenkoetal-PoPoRosubset.

5.3. Experimental procedure

The experiment was conducted in the patient's hospital room at the Center for Neurophysiology Monitoring of the Ghent University Hospital, as they were bedridden during the video-monitoring period.

Patients were sitting upright in their hospital bed in front of the LCD screen at a distance of approximately 60 cm. At the beginning of each trial, a fixation cross appeared in the center of the screen for 1500 ms to inform the subject that a trial was about to start and that they needed to pay attention to the screen. The prime image appeared on the screen for 600 ms, followed by a fixation cross for 650 ms (on average, with a maximal jitter of ±150 ms), followed by the target image for 600 ms. As the jitter was only ±150 ms, it did not influence the presentation speed and none of the participants experienced any problems or even reported noticing any fluctuation in the presentation speed. After the target image, a fixation cross was shown for 1000 ms followed by a semantic association judgment task, during which the patient saw a green tick (representing 'yes') on the left side and a red cross (representing 'no') on the right side of the screen. The subject was instructed to press the left mouse button if (s)he thought the two presented images were semantically related and the right mouse button if otherwise. Note, that the button press moment was delayed to avoid interference between response-related (motor) brain activity and those of interest. Subjects were explicitly instructed to pay attention to the semantic relation of the image pairs, not their visual similarity. The button press accuracies were further used in our behavioral analysis. Prior to the main experiment, all patients completed a training session of four trials in order to familiarize themselves with the task. Each prime-target pair was shown only once. Subjects were given short breaks every 4–5 min. The stimulation was implemented in Matlab, using the Psychophysics toolbox (Brainard, 1997) for precise timing.

5.4. Scalp and invasive EEG acquisition

Simultaneous scalp- and intracranial EEG were recorded from all patients. Scalp EEG was acquired from 27 active electrodes following the 10–20 international system. Conductive gel was applied to each electrode in order to improve the conductance between electrodes and the patient's scalp. Some patients were implanted with both depth and subdural platinum electrodes (Tables S3 and SI), embedded in silastic (Ad-Tech, USA), but in the current study, we focused on data recorded with the subdural grids and strips (ECoG). The contact exposure of the subdural grids was 2.3 mm with a 4 mm contact diameter and a center-to-center distance of 10 mm. The location of each subdural grid and strip is listed in the SI (Table S3 and Fig. S1). Both the scalp- and intracranial EEG of all patients was digitized at a sampling rate of 256 Hz (except for patient P1, where it was 1024Hz) using the medically certified Micromed digital video compatible EEG recording system.

5.5. Localization of ECoG electrodes

Based on the pre-implantation MRI scan of the patient, cortical reconstruction and volumetric segmentation was performed using the Freesurfer image analysis suite (version 6.0) (http://www.freesurfer.net/).

The Freesurfer output was then loaded into Brainstorm (Tadel et al., 2011) and post-implant CT was co-registered with the pre-implant MRI, using the SPM12 (http://www.fil.ion.ucl.ac.uk/spm/) extension. The coordinates of the implanted electrodes were then obtained by visual inspection and mapped onto the cortical surface to account for possible post-implantation brain-shift. For patient P1, no post-implantation CT was available, and the electrode locations were inferred from the artifact on the post-implantation MRI. The electrodes of each subject were transformed to MNI space and manually verified by a neurologist (EK) using the individual subject's cortex and intraoperative images as a reference. For visualization purposes, the obtained MNI coordinates were mapped on a template brain (ICBM 152) provided by the Brainstorm toolbox. The MNI coordinates of each recorded electrode are presented in SI (Table S4).

5.6. Scalp and intracranial EEG data analysis

For scalp-recorded EEG, we conducted an ERP analysis, while for ECoG we conducted three types of analyses: ERP analysis, time-frequency analysis for event-related synchronization/desynchronization (ERS/ERD) and classification analysis for single trial investigation (using ERP epochs, see further).

ERP analysis: The scalp-recorded EEG signal was re-referenced off-line to an average mastoid reference (TP9 and TP10) and filtered twice using a 4th order finite impulse response (FIR) filter: first with a low-pass filter with cutoff at 15 Hz and then with a high-pass filter with cutoff at 0.2 Hz. Then, the signal was segmented into epochs starting 100 ms prior to image onset (primes, related and unrelated targets) until 1000 ms post-onset. In order to clean the obtained epochs from artifacts (eye blink, eye movement or conductance impairment), we set an amplitude threshold of±75 μV on each electrode. Epochs that had a maximum amplitude beyond this threshold at any moment in time were discarded. Only channels that had 30 or more remaining trials after artifact rejection were considered for further analysis. On the remaining epochs, baseline correction was performed using the average EEG signal in the 100 ms

pre-onset time-interval. Here, we evaluated four time-windows reflecting the following ERP components: N100 (50–150 ms), P200 (150–250 ms), N400 (300–500 ms) and P600 (500–800).

For the ECoG recordings, prior to any processing, a specialized epileptologist (co-author AM) checked the recordings and marked the electrodes that exhibited frequent or continuous abnormal activity (interictal or ictal epileptic activity or abnormal slowing). These electrodes were not included in the analysis. For the remaining electrodes, epochs containing interictal or ictal epileptic activity or excessive abnormal slowing were also rejected. To the remaining ECoG data we first applied a conventional ERP analysis, generally identical to the procedure for scalp-recorded EEG, except for the higher epoch rejection threshold ($\pm$500 μV), as in general ECoG data has larger magnitude, and instead of re-referencing to the mastoids, each electrode in each grid was re-referenced to its common average reference (CAR), as usually done in ECoG data analysis (Khachatryan et al., 2018; Wittevrongel et al., 2017).

ERS/ERD analysis: For the ECoG recordings, a time-frequency analysis was performed to mark changes in the spectral power (ERS/ERD) in a given frequency band for particular groups of trials (related, unrelated, prime – no context). Prior to the ERS/ERD analysis, the cleaned raw signal from each grid was re-referenced to its CAR and filtered in three traditional frequency bands (theta: 4–7.5 Hz, alpha: 8–12Hz and high gamma: 80–120 Hz), given their reported relevance in cognitive information processing (Crone et al., 2006). Afterwards, the signal was cut into trials starting 200 ms prior to stimulus onset until 1000 ms post-onset. The ERS/ERD curves for each group were then calculated according to the method described in Pfurtscheller and Lopes da Silva (Pfurtscheller and Lopes da Silva, 1999). First, all epochs belonging to the same class were squared and averaged. The averaged epoch was then baselined to the median activity in the pre-stimulus window, and smoothed using a symmetric 50 ms window ([-25, 25] ms). The 95%-confidence interval was obtained using a bootstrapping procedure with 1000 iterations (Graimann and Pfurtscheller, 2006; Graimann et al., 2002). In each iteration, n data points were randomly selected (with replacement) for each sample and used to ascertain the confidence interval. For each channel, the value of n was set to the minimum number of epochs for the three classes (prime, related target and unrelated target). Note that the value of n varied across channels and subjects as a variable number of epochs were rejected by the expert epileptologist (co-author AM), but was constant within each channel such that the comparison between the classes was unbiased by the number of epochs that were rejected.

Classification analysis: In order to investigate whether single epochs could be identified as belonging to prime, related target or unrelated target, a classification analysis was performed using the spatio-temporal beamformer as classifier. This extension of the original spatial beamformer was introduced for single-trial N400 detection using scalp-recorded EEG (Van Vliet et al., 2016), and since then successfully applied for detecting a wide range of ERP and phase locked scalp-EEG (Wittevrongel and Hulle, 2017), and intracranial responses (Wittevrongel et al., 2018b). In the pertinent study, classification was based on single-trial ERPs (entire 1s epochs). For each stimulus, a stimulus-locked 1-s epoch was extracted, baseline corrected to the average 200 ms pre-stimulus activity, filtered between 0.2 and 15 Hz (using additional pre- and post-epoch data to avoid filtering artifacts), and downsampled to 100 Hz. Classification was applied to each pair of stimulus groups individually (prime vs. related target, prime vs. unrelated target, related vs. unrelated target), using a stratified 5-fold cross-validation approach, and both single-channel and grid/strip-based classification was considered. For a brief description of the mathematical background of the beamformer classifier, we refer to the SI.

5.7. Statistical analysis

As the behavioral data from patient P2 was lost due to technical issues, we analyzed the behavioral data of the remaining 8 subjects using the Kruskal-Wallis non-parametric test in order to account for possible outliers and for the non-normality of the data distribution (checked with the Kolmogorov-Smirnov test) (McDonald, 2014).

We conducted our statistical analysis of the ERP data, for both scalp-recorded and intracranial EEG, with the Kruskal-Wallis test considering stimulus type (related target, unrelated target and prime) as fixed effect. When performing multiple comparisons, we corrected Kruskal-Wallis test results with FDR (3 comparisons per ERP per electrode). We took the average ERP amplitude (area under the curve) in the given time-windows (as defined in section 5.6. on data analysis) as dependent variable and considered a comparison with a (FDR corrected) p-value below 0.05 as statistically significant.

For the significant ERS/ERD (both boundaries of confidence intervals were negative (ERD) or positive (ERS) for 100 ms or longer), we report the average power change across time (APC) compared to the baseline, and the upper and lower boundaries of the confidence interval [CI_{lower} - CI_{upper}].

Finally, we report the outcome of classification analysis in terms of maximum accuracy (in %) for a single electrode and grid.

Author contribution

EK designed and implemented experiment. EC, ID, AM, PB and DVR recruited the patients. AM checked the data on the presence of epileptic and inter-ictal activity. ID and EC provided the extra information on the patients. EK, BW and MFH collected the data. EK and BW conducted analysis and BW generated the figures. EK, BW, MFH and MVH wrote the manuscript. All co-authors equally participated in creating the final draft of the manuscript.

Conflicts of interest

Authors declare no competing interests.

Materials & correspondence

Correspondence and material requests should be addressed to corresponding author.

Acknowledgements

EK and BW are supported by the special research fund of the KU Leuven (C24/18/098). MF is supported by the Hermes Fund of the National Fund for Scientific Research Flanders (SB/151022). MMVH is supported by research grants received from the Financing Program (PFV/10/008), the interdisciplinary research fund (IDO/12/007), the industrial research fund (IOF/HB/12/021) and the special research fund of the KU Leuven (C24/18/098), the Belgian Fund for Scientific Research – Flanders (G088314N, G0A0914N, G0A4118N), the Interuniversity Attraction Poles Programme – Belgian Science Policy (IUAP P7/11), the Flemish Regional Ministry of Education (Belgium) (GOA 10/019), and the Hercules Foundation (AKUL 043).

Appendix A. Supplementary data

Supplementary data to this article can be found online at https://doi.org/10.1016/j.neuroimage.2019.116204.

References

Babajani-feremi, A., et al., 2016. Language mapping using high gamma electrocorticography , fMRI , and TMS versus electrocortical stimulation. Clin. Neurophysiol. 127, 1822–1836.

Badgaiyan, R.D., 2000. Neuroanatomical organization of perceptual Memory : an fMRI study of picture priming. Hum. Brain Mapp. 10, 197–203.

Bar, M., Aminoff, E., 2003. Cortical analysis of visual context. Neuron 38, 347–358.

Başar, E., 1999. Brain Function and Oscillations II. Integrative Brain Function. Neurophysiology and Cognitive Processes. Springer Berlin Heidelberg.
Basar-Eroglu, C., Basar, E., Demiralp, T., Schiirmann, M., 1992. P300-response : possible psychophysiological correlates in delta and theta frequency channels. A review. *Int. J. Psychophysiol.* 13, 161–179.
Bastiaansen, M.C.M., Oostenveld, R., Jensen, O., Hagoort, P., 2008. I see what you mean : theta power increases are involved in the retrieval of lexical semantic information. Brain Lang. 106, 15–28.
Berman, R.A., Colby, C.L., 2002. Spatial working memory in human extrastriate cortex. Physiol. Behav. 77, 621–627.
Binder, J.R., Desai, R.H., Graves, W.W., Conant, L.L., 2009. Where is the semantic system? A critical review and meta-analysis of 120 functional neuroimaging studies. Cerebr. Cortex 19, 2767–2796.
Brainard, D.H., 1997. The psychophysics Toolbox. Spat. Vis. 10, 433–436.
Brouwer, H., Hoeks, J.C.J., 2013. A time and place for language comprehension: mapping the N400 and the P600 to a minimal cortical network. Front. Hum. Neurosci. 7, 758.
Coulson, S., Federmeier, K.D., Van Petten, C., Kutas, M., 2005. Right hemisphere sensitivity to word- and sentence-level context: evidence from event-related brain potentials. J. Exp. Psychol. Learn. Mem. Cogn. 31, 129–147.
Crone, N.E., Sinai, A., Korzeniewska, A., 2006. In Progress in Brain Research, pp. 275–295. https://doi.org/10.1016/S0079-6123(06)59019-3.
Devereux, B.J., Clarke, A., Tyler, L.K., 2018. Integrated deep visual and semantic attractor neural networks predict fMRI pattern-information along the ventral object processing pathway. Sci. Rep. 8.
DiCarlo, J.J., Zoccolan, D., Rust, N.C., 2012. How does the brain solve visual object recognition? Neuron 73, 415–434.
Eddy, M.D., Schnyer, D., Schmid, A., Holcomb, P.J., 2007. Spatial dynamics of masked picture repetition effects. Neuroimage 34, 1723–1732.
Gevins, A., Smith, M.E., Mcevoy, L., Yu, D., 1997. High-resolution EEG mapping of cortical activation related to working Memory : effects of task difficulty , type of processing , and practice. Cerebr. Cortex 7, 374–385.
Ghosh Hajra, S., et al., 2018. Multimodal characterization of the semantic N400 response within a rapid evaluation brain vital sign framework. J. Transl. Med. 16, 1–11.
Gonzalez, A., et al., 2015. Electrocorticography reveals the temporal dynamics of posterior parietal cortical activity during recognition memory decisions. Proc. Natl. Acad. Sci. 112, 11066–11071.
Graimann, B., Pfurtscheller, G., 2006. Quantification and visualization of event-related changes in oscillatory brain activity in the time–frequency domain. Prog. Brain Res. 159, 79–97.
Graimann, B., Huggins, J.E., Levine, S.P., Pfurtscheller, G., 2002. Visualization of significant ERD/ERS patterns in multichannel EEG and ECoG data. Clin. Neurophysiol. 113, 43–47.
Halgren, E., et al., 1994. Spatio-temporal stages in face and word processing. 2. Depth-recorded potentials in the human frontal and Rolandic cortices. J. Physiol. - Paris 88, 51–80.
Harel, A., Kravitz, D.J., Baker, C.I., 2014. Task context impacts visual object processing differentially across the cortex. Proc. Natl. Acad. Sci. 962–971. https://doi.org/10.1073/pnas.1312567111.
Hart, M.A., Reeve, T.G., 2007. Equivalency of reaction times for simple and primed tasks. Acta Psychol. (Amst). 125, 291–300.
Haufe, S., et al., 2018. Elucidating relations between fMRI , ECoG and EEG through a common natural stimulus. Neuroimage 179, 79–91.
Heyman, T., Van Rensbergen, B., Storms, G., Hutchison, K.A., Deyne, S. De, 2015. The influence of working memory load on semantic priming. J. Exp. Psychol. Learn. Mem. Cogn. 41, 911–920.
Infarinato, F., et al., 2015. On-going frontal alpha rhythms are dominant in passive state and desynchronize in active state in adult gray mouse lemurs. November PLoS One 3, 1–20.
Jackson, R., Lambon, Ralph, Matthew, A., Pobric, G., 2015. The timing of anterior temporal lobe involvement in semantic processing. J. Cogn. Neurosci. 27, 1388–1396.
James, T.W., Humphrey, G.K., Gati, J.S., Menon, R.S., Goodale, M.A., 2000. The effects of visual object priming on brain activation before and after recognition. Curr. Biol. 10, 1017–1024.
Kapeller, C., Ogawa, H., Schalk, G., Kunii, N., Coon, W.G., 2018. Real-time detection and discrimination of visual perception using electrocorticographic signals. J. Neural Eng. 15, 1–16.
Khachatryan, E., Camarrone, F., Fias, W., Van Hulle, M.M., 2016. Event related potential response unveils effect of second language manipulation on first language processing. PLoS One 11, 1–26.
Khachatryan, E., et al., 2016. Cortical distribution of N400 potential in response to semantic priming with visual non-linguistic stimuli. In: IEEE Workshop on Statistical Signal Processing (SSP).
Khachatryan, E., et al., 2018. A new insight into sentence comprehension: the impact of word associations in sentence processing as shown by invasive EEG recording. Neuropsychologia 108, 103–116.
Kiefer, M., 2001. Perceptual and semantic sources of category-specific effects : event-related potentials during picture and word categorization. Mem. Cogn. 29, 100–116.
Klimesch, W., 2012. Alpha-band oscillations, attention, and controlled access to stored information. Trends Cogn. Sci. 16, 606–617.
Kovalenko, L.Y., Chaumon, M., Busch, N.A., 2012. A pool of pairs of related objects (POPORO) for investigating visual semantic integration: behavioral and electrophysiological validation. Brain Topogr. 25, 272–284.
Kravitz, D.J., Saleem, K.S., Baker, C.I., Ungerleider, L.G., Mishkin, M., 2013. The ventral visual pathway: an expanded neural framework for the processing of object quality. Trends Cogn. Sci. 17, 26–49.
Kutas, M., Federmeier, K., 2009. N400. Scholarpedia, 4, p. 7790.
Kutas, M., Federmeier, K.D., 2011. Thirty years and counting: finding meaning in the N400 component of the event-related brain potential (ERP). Annu. Rev. Psychol. 62, 621–647.
Lau, E.F., Gramfort, A., Hämäläinen, M.S., Kuperberg, G.R., 2013. Automatic semantic facilitation in anterior temporal cortex revealed through multimodal neuroimaging. J. Neurosci. 33, 17174–17181.
Lucia, M. De, et al., 2010. Perceptual and semantic contributions to repetition priming of environmental sounds. Cerebr. Cortex 20, 1676–1684.
Luck, S.J., 2005. An Introduction to Event Related Potential Technique. Monographs of the Society for Research in Child Development, 79. MIT Press, MA.
Martinovic, J., Lawson, R., Craddock, M., 2012. Time course of information processing in visual and haptic object classification. Front. Hum. Neurosci. 6, 1–11.
McDonald, J.H., 2014. In Handbook of Biological Statistics 157–164. Sparky House Publishing.
Mellema, M.S., Friedmana, R.B., Medvedev, A.V., 2013. Gamma- and theta-band synchronization during semantic priming reflect local and long-range lexical-semantic networks. Brain Lang. 127, 1–27.
Migliaccio, R., Boutet, C., Valabregue, R., Ferrieux, S., 2016. The brain network of Naming : a lesson from primary progressive aphasia. PLoS One 1–17. https://doi.org/10.1371/journal.pone.0148707.
Miller, K.J., Weaver, K.E., Ojemann, J.G., 2009. Direct electrophysiological measurement of human default network areas. Proc. Natl. Acad. Sci. 106, 12174–12177.
Mummery, C.J., et al., 1999. Disrupted temporal lobe connections in semantic dementia. Brain 122, 61–73.
Nobre, a C., McCarthy, G., 1995. Language-related field potentials in the anterior-medial temporal lobe: II. Effects of word type and semantic priming. J. Neurosci. 15, 1090–1098.
Nyhus, E., Curran, T., 2010. Functional role of gamma and theta oscillations in episodic memory. Neurosci. Biobehav. Rev. 34, 1023–1035.
Parvizi, J., Kastner, S., 2018. Promises and limitations of human intracranial electroencephalography. Nat. Neurosci. 21, 474–483.
Patterson, K., Nestor, P.J., Rogers, T.T., 2007. Where do you know what you know ? The representation of semantic knowledge in the human brain. Nat. Rev. Neurosci. 8, 976–988.
Pfurtscheller, G., Lopes da Silva, F.H., 1999. Event-related EEG/MEG synchronization and desynchronization : basic principles. Clin. Neurophysiol. 110, 1842–1857.
Proverbio, A.M., Del Zotto, M., Zani, A., 2007. The emergence of semantic categorization in early visual processing : ERP indices of animal vs . artifact recognition. BMC Neurosci. 8, 1–16.
Rangarajan, V., et al., 2014. Electrical stimulation of the left and right human fusiform gyrus causes different effects in conscious face perception. J. Neurosci. 34, 12828–12836.
Riès, S.K., et al., 2017. Spatiotemporal dynamics of word retrieval in speech production revealed by cortical high-frequency band activity. Proc. Natl. Acad. Sci. 4530–4538. https://doi.org/10.1073/pnas.1620669114.
Rossell, S.L., Price, C.J., Nobre, A.C., 2003. The anatomy and time course of semantic priming investigated by fMRI and ERPs. Neuropsychologia 41, 550–564.
Rupp, K., et al., 2017. NeuroImage Semantic attributes are encoded in human electrocorticographic signals during visual object recognition. Neuroimage 148, 318–329.
Sabb, F.W., Bilder, R.M., Chou, M., Bookheimer, S.Y., 2007. Working memory effects on semantic processing : priming differences in pars orbitalis. Neuroimage 37, 311–322.
Schacter, D.L., Dobbins, I.G., Schnyer, D.M., 2004. Specificity of Priming : a cognitive neuroscience perspective. Nat. Rev. Neurosci. 5, 853–862.
Tadel, F., Baillet, S., Mosher, J.C., Pantazis, D., Leahy, R.M., 2011. Brainstorm: a user-friendly application for MEG/EEG analysis. Comput. Intell. Neurosci. 2011.
Thesen, T., et al., 2012. Sequential then interactive processing of letters and words in the left fusiform gyrus. Nat. Commun. 3, 1–19.
Thoma, V., Henson, R.N., 2011. Object representations in ventral and dorsal visual streams: fMRI repetition effects depend on attention and part–whole configuration. Neuroimage 57, 513–525.
Tivarus, M.E., Ibinson, J., Hillier, A., Schmalbrock, P., Beversdorf, D.Q., 2007. An fMRI study of semantic priming: modulation of brain activity by varying semantic distances. Cogn. Behav. Neurol. 19, 194–201.
Tomassini, A., Ambrogioni, L., Medendorp, W.P., Maris, E., 2017. Theta oscillations locked to intended actions rhythmically modulate perception. Elife 6, 1–18.
Towle, V.L., et al., 2008. ECoG gamma activity during a language task : differentiating expressive and receptive speech areas. Brain 131, 2013–2027.
Van Vliet, M., et al., 2014. Response-related potentials during semantic priming: the effect of a speeded button response task on ERPs. PLoS One 9.
Van Vliet, M., et al., 2016. Single-trial ERP component analysis using a spatio-temporal LCMV beam former. IEEE Trans. Biomed. Eng. 63, 55–66.
Wittevrongel, B., Hulle, M. M. Van, 2017. Spatiotemporal Beamforming : a transparent and unified decoding approach to synchronous visual. Brain-Computer Interfacing 11, 1–12.
Wittevrongel, B., et al., 2017. Representation of steady-state visual evoked potentials elicited by luminance flicker in human occipital cortex: an electrocorticography study. Neuroimage 175, 315–326.

Wittevrongel, B., et al., 2018. Representation of steady-state visual evoked potentials elicited by luminance flicker in human occipital cortex: an electrocorticography study. Neuroimage 175.
Wittevrongel, B., Khachatryan, E., Hnazaee, M.F., 2018. Decoding Steady-State Visual Evoked Potentials from Electrocorticography, 12, pp. 1–14.
Xu, M., Lauwereyns, J., Iramina, K., 2012. Dissociation of category versus item priming in face processing : an event-related potential study. Cogn. Neurodyn. 6, 155–167.
Zhanga, X.L., Begleiterb, H., Porjeszb, B., Litkeb, A., 1997. Visual object priming differs from visual word priming : an ERP study. Electroencephalogr. Clin. Neurophysiol. 102, 200–215.